Blue-Green Systems

IWA PUBLISHING

Blue-Green Systems Vol 5 No 2, 152 doi: 10.2166/bgs.2023.027

Modeling bioinfiltration surface dynamics through a hybrid geomorphic-infiltration model

Richard Ampomah[a], Danielle Holt[a], Cole Smith[a], Virginia Smith [a,*], Kristin Sample-Lord[a] and Jonathan Nyquist[b]

[a] Department of Civil and Environmental Engineering, Villanova University, Villanova, PA, USA
[b] Geophysics, Earth & Environmental Science, Temple University, 1901 N. 13th St., Philadelphia, PA 19122, USA
*Corresponding author. E-mail: virginia.smith@villanova.edu

VS, 0000-0002-5640-8692

ABSTRACT

Bioinfiltration systems are an increasingly prevalent mechanism for urban stormwater mitigation. One major challenge for the sustainability of bioinfiltration systems is erosion and channelization due to high bed shear stresses developed during large storm events. Sedimentation within these systems could also impact their performance as fine sediment may clog pathways necessary for infiltration. Understanding the geomorphology, shear stress, and sediment flux in the system can help predict maintenance needs associated with erosion and deposition. The current study introduces a framework for addressing this problem by combining a sediment transport model, FaSTMECH, with the Green-Ampt infiltration model. A comparison of observed and predicted ponding depths shows very good agreement (median Nash–Sutcliffe efficiency coefficient = 0.93) and demonstrates the ability of this novel framework in predicting the hydraulics and morphology within a bioswale bioinfiltration system. The framework introduced in this study opens the door to understanding sediment transport dynamics within a bioswale, which has the potential to advance planning and design to minimize impacts due to excessive erosion or deposition within bioswale bioinfiltration systems.

Key words: best management practices (BMPs), green infrastructure, infiltration, sediment transport, storm water management, surface water hydrology

HIGHLIGHTS

- Sedimentation is a major challenge to maintaining urban bioinfiltration systems.
- Sediment transport is modeled by a hydro-geomorphic model.
- The model is run and calibrated with a unique dataset of observations from a bioswale bioinfiltration system.
- Predicting areas of erosion and deposition allows for the identification of areas at risk.

NOTATION

C_d	drag coefficient
D	median particle size
F	accumulated depth of infiltrated water
P	pressure
Rep	particle Reynolds number
R	submerged specific gravity
U	velocity vector
f	infiltration rate
g	gravitational acceleration
h	mean flow depth
k_{sat}	saturated hydraulic conductivity
n	Manning's roughness coefficient
t	time
q^*	dimensionless bed transport rate
φ	wetting front suction head

θ moisture content
ρ density of water
ν kinematic viscosity
τ^* dimensionless shear stress
τ_c^* dimensionless critical shear stress (shield parameter)
ρ_s density of sediment

INTRODUCTION

Urbanization and the creation of impervious surfaces typically result in increased stormwater runoff, elevated risk of flooding, and instability in urban streams due to substantial bank erosion (Wolman & Schick 1967; Leopold 1968; Hammond *et al.* 2015; Anim & Banahene 2021). These drastic changes within watersheds and the associated water quality problems in urban streams often have far-reaching consequences such as disruption of the stream's ecosystem and disconnection from the floodplain (McGrane 2016; Waite *et al.* 2019). Over the past two decades, innovations in urban stormwater engineering have led to the implementation of stormwater management practices (SMPs) such as bioinfiltration systems. Such systems are effective in reducing runoff volume resulting in less impactful stormwater runoff discharge into receiving water bodies (Davis *et al.* 2012; Lee *et al.* 2016). Bioinfiltration systems have also been shown to be beneficial for significant water quality improvements for both organic and inorganic pollutants (Davis *et al.* 2003, 2009; Jeon *et al.* 2021). The bioinfiltration system's ability to treat total suspended solids (TSS) is particularly effective as a significant quantity of sediment is retained in these systems (Smith *et al.* 2023). The latter aid municipalities in meeting environmental regulations, resulting in bioinfiltration systems becoming an increasingly important and pervasive feature in the urban landscape. Computational modeling creates an exciting stage for innovation and a deeper understanding of these nature-based systems within the built environment.

The performance of the system over time can be heavily impacted by erosion or deposition of significant amounts of sediment (DelGrosso *et al.* 2019). In recent years, there has been a growing interest in understanding the impact of sedimentation on the performance of bioinfiltration systems to ensure the sustainable function of the infrastructure (Coustumer *et al.* 2012; DelGrosso *et al.* 2019; Homet *et al.* 2022). Sediment removal can lead to one of the most expensive maintenance costs associated with bioinfiltration systems (Hunt *et al.* 2020). Clay and silt-sized particles within suspended sediment can lead to clogging the infiltration media and reduce the saturated hydraulic conductivity (k_{sat}) of the soil (Langergraber *et al.* 2003; Asleson *et al.* 2009; Virahsawmy *et al.* 2014). Many jurisdictions have thus implemented SMP manuals or design standards aimed at mitigating erosion, channelization, and sedimentation within these systems (e.g., Philadelphia Water Department 2021).

Prior studies regarding bioinfiltration soil media have primarily focused on the reduction of k_{sat} as a result of the introduction of sediment (Gonzalez-Merchan *et al.* 2010; Coustumer *et al.* 2012) and not on the surficial movement of sediment. However, the ability to link bioinfiltration to surface morphology is crucial for a more sustainable design and can open the door to targeted maintenance strategies for such systems. This is particularly true for specific geometries of bioinfiltration systems, such as those designed for conveyance. Specifically, understanding the shear stress distribution and sediment flux within a system allows for a more effective prioritization of maintenance of systems with a high risk of failure or underperformance due to sedimentation or erosion.

Existing models for sediment transport, such as the ROWERO (Wu & Meyer 1989) and the surface irrigation model by Mailapalli *et al.* (2013), are better suited for irrigation furrows, not a vegetated bioinfiltration basin. Currently, geomorphic models do not exist for bioinfiltration systems; however, advancements in fluvial geomorphic modeling (Nelson 2018) provide a starting point for modeling sediment flux in bioinfiltration. There are challenges in applying fluvial geomorphic models to bioinfiltration because they do not account for the high infiltration rates typical in such systems. Infiltration within bioinfiltration systems constitutes a significant volume of water removal (Davis *et al.* 2009) and, therefore, cannot be ignored when estimating hydrographs or predicting geomorphic changes.

The International River Interface Cooperative Software (iRIC) (Nelson 2018) is a public domain software platform for numerical simulation of river flow and morphodynamics. The iRIC platform hosts a number of two- and three-dimensional solvers for flow, sediment transport, and bed evolution modeling, and has the advantage of both pre- and post-processing of input and results, respectively (Nelson *et al.* 2010). The flow and sediment transport with morphologic evolution of channels (FaSTMECH) (Nelson *et al.* 2003), one of the river modeling packages hosted on the iRIC platform, has been successfully implemented in a variety of studies including

predicting morphological alterations in backwater zones in rivers (Hosseiny & Smith 2019), quantifying and visualizing uncertainty associated with flood inundation maps (Zarzar *et al.* 2018), explaining spatial patterns of mussel beds (May & Pryor 2015), investigating chute formation along meandering streams (Harrison *et al.* 2015), and modeling the effects of flow and sediment transport on fish spawning habitat (McDonald *et al.* 2010; McKean & Tonina 2013). This model was chosen for modeling the bioretention due to the available solvers and its ability to represent flow and sediment transport in two dimensions.

Here, we present a novel framework for analyzing sediment dynamics within a bioinfiltration system. This new framework combines the Green-Ampt infiltration equation (Green & Ampt 1911) with the FaSTMECH sediment transport model for an estimation of both infiltration and sediment transport. The advantage of using a Green-Ampt infiltration model is its wide acceptability as a suitable infiltration model for bioinfiltration systems, with easily obtainable input parameters compared with other infiltration models (Bedient *et al.* 2008).

This study introduces a predictive framework for identifying potential high shear stress (erosion) and high sediment deposition (sedimentation) areas within a bioinfiltration system, which will allow for prioritizing areas in design and maintenance. By integrating different mechanistic models iteratively, a representation of bioinfiltration surface dynamics can be produced (Chappell *et al.* 2006; Lastra *et al.* 2008). The increasing availability of open-access sediment models and several well-established infiltration models makes this approach computationally less expensive and more feasible (Garcia 2007). The objective of this study is to create a framework to examine morphology within a bioswale bioinfiltration system to identify areas at risk of sedimentation or erosion through combining an existing fluvial geomorphic modeling tool with a widely accepted infiltration model.

METHODS

Study area

As part of the Pennsylvania Department of Transportation (PennDOT) Girard Avenue Interchange expansion of the Interstate-95 (I-95) in Philadelphia, PA, USA, several SMPs are under construction to mitigate the additional runoff generated due to the I-95 highway expansion. In partnership with Villanova University, a few of these sites are currently being studied to inform the design of additional units in the next phases of the project. The current study focuses on SMP A shown in Figure 1. SMP A is a bioswale configuration of a bioinfiltration system constructed in 2015 and connected to the Philadelphia combined sewer system (CSS). This site was selected for this study as it has a substantial record of flow and ponding data for modeling. It has a total length of 150 m, which is divided into three subbasins by two weirs. The lower subbasin is 66 m long; the upper and middle subbasins are each 42 m long. The upper and lower subbasins have a 0.6 m (2 ft) thick layer of sandy loam as the infiltration soil media (Smith *et al.* 2021). The lower subbasin was the focus of the current study as its configuration is the most suitable for this research due to inflow and outflow conditions aligning with the boundary condition requirements for model hydraulics solver. The configuration of SMP A has two dividing weirs and multiple lateral inflows, coming from the three 18-inch inlets.

Data assimilation

Inflow

Flow into SMP A was monitored by a Blue Siren area/velocity flow sensor installed at all three inlets. Internal flow depth was monitored by a CS451 pressure transducer installed upstream of each weir. Flow measurements were recorded at 5-min intervals from the beginning of each storm event. The combined flows from the N10 inlet and the downstream weir were used in the simulation (Figure 1). Rainfall data were collected from a tipping bucket rain gage located at the southern end of the site. The study used data collected between May 2017 and April 2019 for simulation and model verification. For the purposes of hydraulic simulation, each hydrograph was treated as a separate event. An event was considered to have ended when the flow of the hydrograph goes to zero. The next event is considered as the next non-zero period. This discretization was necessary for computational efficiency considering the hydrographs have such a high temporal resolution. A total of 619 events between May 2017 and April 2019 were analyzed. The number of events was trimmed down to 100 to exclude events with peak discharge less than 0.0002 m^3/s because they did not produce a shear stress that was geomorphically significant (these events are summarized in Table S.1 of the Supplemental Information). This threshold was established by estimating the critical shear stress for the median soil (particle d_{50}) and estimating the corresponding critical discharge. Assumptions made in establishing this threshold are later explained.

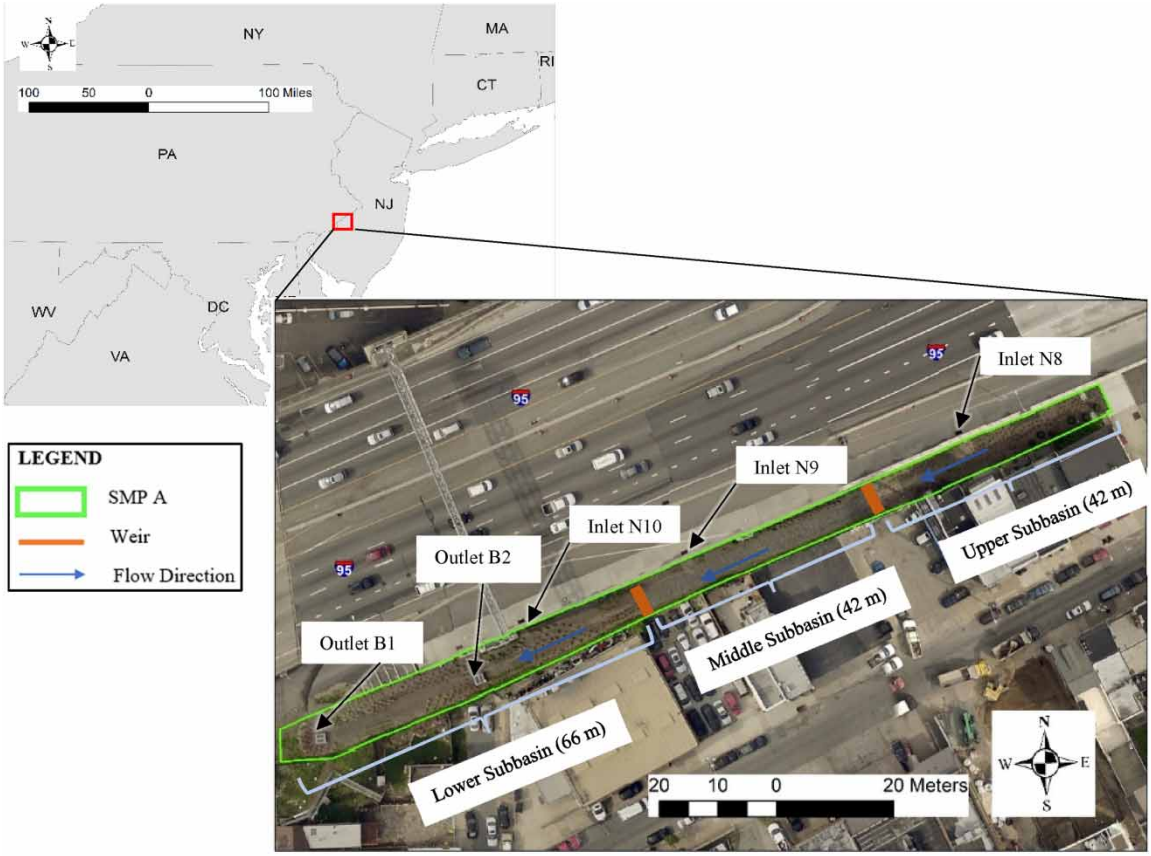

Figure 1 | Study site location of stormwater management practice (SMP) A along Interstate 95 in Philadelphia, PA (created using ArcGIS® software by Esri).

Geometry

The simulation was based on a high-resolution terrestrial Light Detection And Ranging (LiDAR) Digital Elevation Model (DEM) with a pixel size of 0.1 m × 0.1 m collected in the summer of 2017 (Figure 2). These data were collected using a Trimble TX-5 terrestrial LiDAR scanner and processed with Trimble Realworks. Reflections from vegetation were removed from the point cloud using LAStools (http://lastools.org/). Las-ground was used to classify ground points. These points were used to create the final DEM through the Quick Terrain Modeler (https://appliedimagery.com/) for a final quality control of the ground points and to export the DEM.

This high resolution of DEM allows an accurate estimation of the hydraulic parameters required for a reliable evaluation of morphology within the bioinfiltration system. The DEM was modified to include the location of the two outlet structures within the model domain. Computation in FastMECH was performed on a 0.3 m-by-0.4 m grid, which was determined to be a computationally efficient grid size for this study (smaller grids were not feasible due to instabilities in the model).

Infiltration

Infiltration constitutes an important component of the flow mass balance within a bioinfiltration system and cannot be ignored in evaluating bioinfiltration system hydraulics. However, there are currently no known geomorphic models which account for the high infiltration rates typical of bioinfiltration systems (e.g., 0.6–25 cm/h; Philadelphia Water Department 2021) such as SMP A. This study introduces a new approach for bioinfiltration system geomorphic simulation which employs an upfront accounting for infiltration using the Green-Ampt model (Green & Ampt 1911). The Green-Ampt infiltration model (Equations (1) and (2)) was chosen for this study because it is a widely accepted method for modeling infiltration of stormwater in bioinfiltration systems and requires input parameters that can be measured or easily estimated from literature (Bedient *et al.* 2008). The Green and Ampt

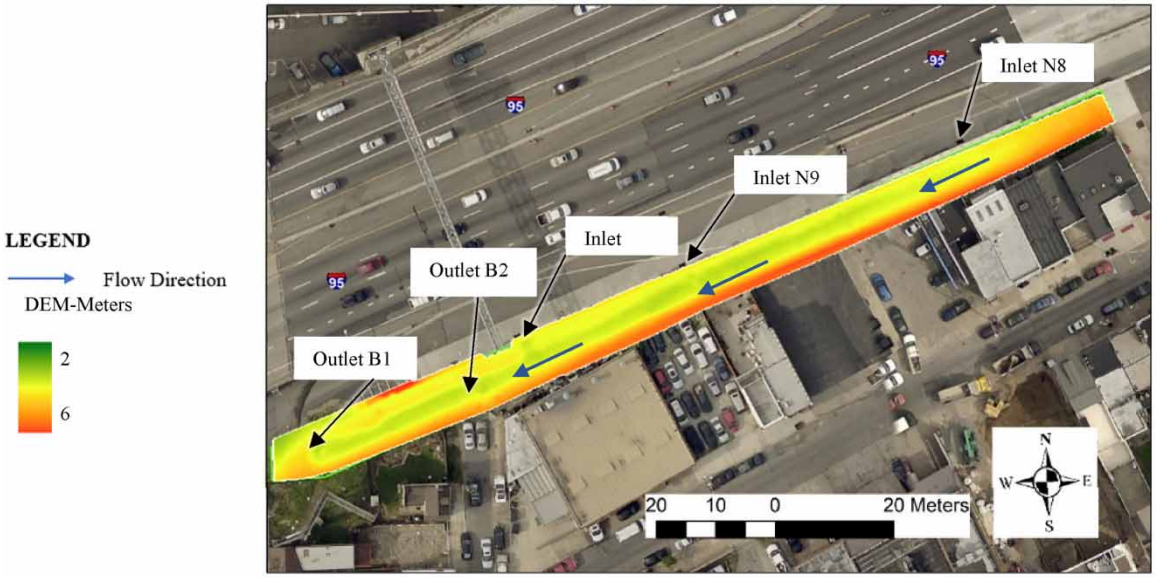

Figure 2 | Study site location of stormwater management practice (SMP) A along Interstate 95 in Philadelphia, PA.

infiltration model is defined as

$$F(t) = k_{\text{sat}}t + \varphi\Delta\theta\ln\left(1 + \frac{F(t)}{\varphi\Delta\theta}\right) \tag{1}$$

in which

$$f = \left(1 + \frac{\varphi\Delta\theta}{F}\right) \tag{2}$$

where $F(t)$ is the accumulated depth (m) of infiltrated water as a function of time, t (s), k_{sat} is the saturated hydraulic conductivity (m/s), ψ is the wetting front suction head (m), $\Delta\theta$ is the change in volumetric water content as the wetting front passes a point within the soil column, and f is the infiltration rate (m/s). Simplifying assumptions included in the Green-Ampt infiltration model include a sharp wetting front, soil with homogenous water retention and transmission properties, suction at the wetting front remains constant, and soil behind the wetting front is uniformly wet (Tindall *et al.* 1999).

The initial volumetric water content of the soil (θ_i) and the saturated volumetric water content (θ_s) are required to determine $\Delta\theta$. Values of θ_s are often assumed equal to the soil porosity, f. In this study, values of f and φ were initially estimated based on recommendations by Rawls *et al.* (1983) for loamy sand. Porosity values were confirmed through comparison with measurements from soil cores collected from the field. When data on the initial water content of the soil prior to each storm event were unavailable, θ_i was assumed equal to the field capacity (the θ of the soil after excess water has drained). Average assumed values for f, field capacity, and φ were 0.4, 0.14, and 6.13 cm, respectively.

Previous studies have shown that k_{sat} values play the most significant role in modeling infiltration rates of stormwater control measures using the Green-Ampt method, with less sensitivity to other input parameters such as ψ or $\Delta\theta$ (Weiss & Gulliver 2015). In addition, the presence of vegetation and activities of other organisms within the soil are known to impact *in situ* infiltration rates and may result in a higher performance of the system. Therefore, the field k_{sat} and influence of vegetation were investigated through field infiltration testing. Spot-infiltration tests were performed with an automated SATURO dual head infiltrometer (METER Group, Inc. USA). Infiltration tests were performed at multiple locations throughout the SMP along the basin centerline to obtain a representative geometric mean k_{sat} for the basin. Values of k_{sat} from field spot-infiltration tests can be highly spatially variable and typically are log-normally distributed, supporting the use of a geometric mean of the measured k_{sat} values as the overall representative k_{sat} for the basin (Ebrahimian *et al.* 2019). Press (2019)

recommended that, for testing of bioinfiltration sites with infiltrometers such as the SATURO, spot-infiltration tests should be performed at a minimum of five locations to obtain a geometric mean k_{sat} representative of the basin. Thus, the geometric mean k_{sat} values in this study were based on the results of infiltration tests performed at at least five locations throughout the basin. Each of the k_{sat} values measured in the field was temperature corrected. The geometric mean k_{sat} for the field spot-infiltration measurements was 5 cm/h.

In addition, ponding level was continuously monitored in the field with a level sensor located near the B2 outlet structure (Campbell Scientific CS451). The sensor had a total error band of ± 2 mm. Monitoring occurred from May 2017 to April 2019. For all storm events during that period that produced a response from the level sensor, a curve fitting function was applied to the 5-min ponding data to calculate an average recession rate during the recession limb when rainfall was not occurring. The average recession rate was 6 cm/h. However, the measured water levels near the gage at the B2 outlet structure did not necessarily represent the average water level throughout the SMP. This information was used to calibrate the hydraulics of the model.

To allow for comparison with the results of the field-measured k_{sat} from the infiltration testing, hydraulic conductivity tests were performed in the laboratory on 3.8-cm-long soil cores collected from the field. The laboratory k_{sat} was measured under constant-head conditions in general accordance with ASTM D2434. The average hydraulic gradient during testing was 5. For all of the laboratory tests, permeation continued until at least four consecutive values of the ratio of outflow to inflow were between 0.75 and 1.25, and at least four consecutive k_{sat} values were within $\pm 25\%$ of the mean k_{sat} value of the consecutive measurements. The mean k_{sat} based on the laboratory testing was 3 cm/h, which was lower than the field k_{sat} of 5 cm/h. However, the lower k_{sat} value observed for the laboratory testing was expected, as laboratory measurements on smaller samples do not account for the presence of roots and other macropore effects present in the field. Thus, as the field infiltration measurements were considered more representative of actual infiltration conditions, a k_{sat} value of 5 cm/h was used in the analysis.

For each storm, the result of the Green-Ampt infiltration rate was converted to a volume rate by multiplying with the surface area of the study area (240 m^2). Using the estimated volumetric infiltration rate, the storm events were filtered further to only include the significant storm events (events greater than the estimated minimum volumetric infiltration rate, 0.003 m^3/s). 66 such significant storm events were identified in this study. The excess runoff was computed as the difference between infiltration and inflow hydrograph, which was then used for the geomorphic simulation (shown in Figure 3).

Ponding depth

In addition to the inflow hydrographs, ponding depth (Figure 4) was measured at the two outlet structures (B1 and B2). Ponding depth from the B1 gage was utilized in setting the downstream boundary condition of the model. Ponding data obtained from the B2 gage were used for model verification and for estimating the system's recession rates previously discussed.

Modeling

The model used an iterative process described in Figure 5. The framework developed in this study uses the iRIC software for its hydraulic and geomorphic simulation. The iRIC platform hosts a solver for two- and three-dimensional flow, sediment transport, and bed evolution modeling (Nelson *et al.* 2010). The FaSTMECH (Nelson *et al.* 2003) modeling package hosted on the iRIC platform was used due to its high efficiency and easy setup for quasi-steady flow and sediment transport simulation.

Governing equations

Geomorphic simulation within FaSTMECH is preceded by hydraulic calculations to ascertain parameters such as flow depths, velocities, and bed shear stresses. The hydraulic calculations are governed by the Navier–Stokes equations (Equations (3) and (4)) which characterize the relationship between pressure, density, and velocity of a moving fluid. These continuity and momentum equations (Navier–Stokes) are given as

$$\nabla \cdot U = 0 \tag{3}$$

$$\frac{\partial U}{\partial t} + U \cdot \nabla U = -\frac{1}{\rho}\nabla P + g + \nu \nabla^2 U \tag{4}$$

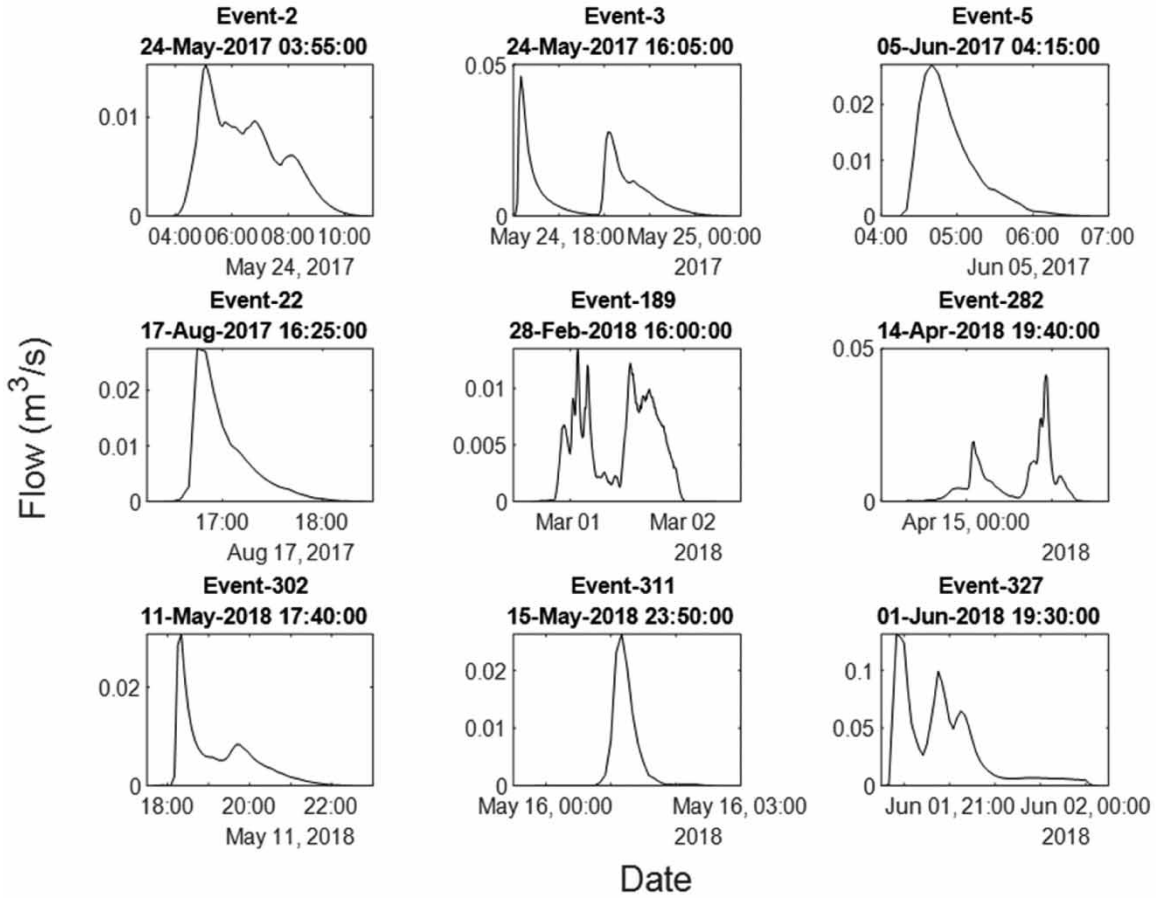

Figure 3 | A sample of the total hydrographs representing individual storm events used in the analysis.

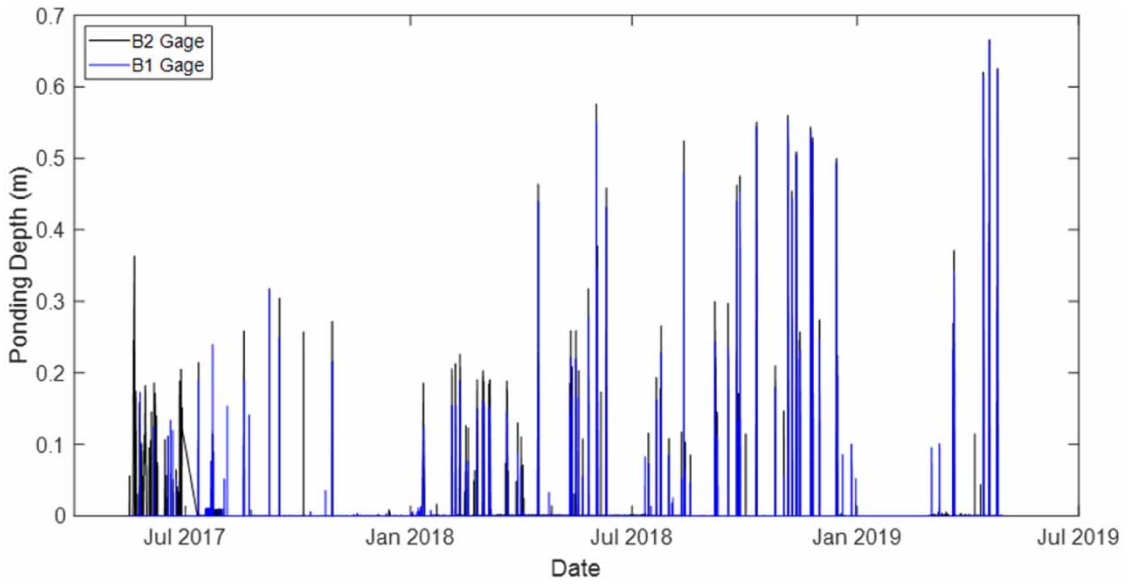

Figure 4 | Measured ponding depth at the B1 and B2 gage stations.

where $\boldsymbol{U}$ represents the velocity vector in the X, Y, and Z dimensions, ρ is the density of the fluid, P is the pressure, ν is the kinematic viscosity, and g is the gravitational acceleration. Due to challenges with solving the full form of these equations, most numerical models for fluid flow such as FaSTMECH use an averaged version of these equations known as the Reynolds-averaged Navier–Stokes equations, a modified form of the Navier–Stokes Equations for the mass and momentum of fluid flow (Jarman *et al.* 2008; Nelson 2016).

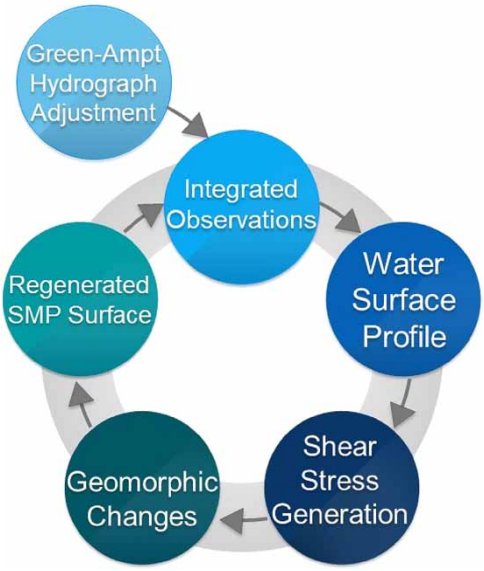

Figure 5 | The modeling workflow process.

The Yalin (1963) sediment transport model was used for the geomorphic aspects of the simulation. The Yalin sediment transport function is considered the most reliable for modeling shallow channel flow and is well suited for particles sizes represented in this study (Garcia 2007). The median particle size (d_{50}) based on 17 samples collected from the lower subbasin was 0.62 mm (Smith *et al.* 2021). The Yalin transport function is given as

$$q^* = 0.635s(\tau^*)^{1/2}\left[1 - \frac{\ln(1 + a_2 s)}{a_2 s}\right] \tag{5}$$

$$a_2 = 2.45(R+1)^{-0.4}(\tau_c^*)^{1/2}, \quad s = \frac{\tau^* - \tau_c^*}{\tau_c^*} \tag{6}$$

where q^* is the dimensionless bed transport rate, τ^* is the dimensionless shear stress, τ_c^* is the dimensionless critical shear stress or Shields parameter, and R is the submerged specific gravity of the sediment.

Boundary conditions

A boundary condition was defined for the upstream and downstream ends of the modeling domain. The downstream boundary condition was set using ponding depth measurements from the B1 gage. The upstream boundary condition was specified as a hydrograph. As FaSTMECH only allows for a single upstream boundary, the two upstream flows were combined into one total inflow hydrograph.

Surface roughness from vegetation

Roughness was specified as a drag coefficient corresponding to a Manning's roughness value of 0.03. This Manning's roughness value was based on a recommendation by Arcement & Schneider (1989) for a straight sand bed channel with scattered vegetative covering. Drag coefficient is defined as

$$C_d = \frac{n^2 g}{h^{1/3}} \tag{7}$$

in which C_d is the drag coefficient, n is the Manning's roughness value, h is the mean flow depth, and g is the gravitational acceleration. Using a mean flow depth (h) of 0.2 m (Figure 4), the estimated C_d was 0.02.

Incipient motion

The critical shear stress necessary for morphology within SMP A was determined to be 0.32 Pa for a particle d_{50} of 0.62 mm. The critical shear stress was estimated based on the Brownlie (1981) equation, which provides a good

fit for Shield's diagram for incipient motion. Brownlie's equation is defined as

$$\tau_c^* = 0.22\mathrm{Rep}^{-0.6} + 0.06\exp(-17.77\mathrm{Rep}^{-0.6}) \tag{8}$$

$$\mathrm{Rep} = \sqrt{gRD} \times \frac{D}{v} \tag{9}$$

$$R = \frac{\rho_s}{\rho} - 1 \tag{10}$$

where D is the median particle size, g is the gravitational acceleration, R is the submerged specific gravity, Rep is the Particle Reynold's number, τ_c^* is the dimensionless critical shear stress (Shields parameter), v is the kinematic viscosity of water, ρ is the density of water, and ρ_s is the density of sediment. The critical shear stress is estimated from the dimensionless critical shear stress by multiplying by a factor of ρgRD. With a critical shear stress of 0.32 Pa, the critical discharge necessary for sediment transport within SMP A was determined as 0.0002 m^3/s.

Model validation

To quantify the accuracy of the prediction framework, two statistics were computed for each comparison of observed and predicted ponding depth: the Nash–Sutcliffe efficiency (NSE) coefficient and the correlation coefficient (CC) (Supplementary Material, Table S1). The NSE (Nash & Sutcliffe 1970) is commonly used for assessing the predictive power of hydrologic models. The NSE has a range of $-\infty$ to 1 with a value of 1 representing a perfect match. A negative NSE value indicates that the observed mean is a better predictor than the model. The CC measures the linear correlation between the observed and predicted results.

RESULTS AND DISCUSSION

Hydrologic and hydraulic simulation

A novel framework for geomorphology within conveyance bioinfiltration systems is introduced, a hybrid approach which combines the widely accepted Green-Ampt infiltration model with a sediment transport model. Incorporating the Green-Ampt infiltration model allowed for a more accurate determination of the excess runoff hydrograph. Based on the assumed porosity, field capacity, and wetting front suction head for loamy sand soil, the estimated minimum infiltration volume rate was 0.003 m^3/s (Figure 6). In Figure 6, it is notable that the infiltration volume rate is constant throughout the span of each event. A plot of the infiltration volume rate on a larger scale shows a rapid decline from the initial infiltration volume rate to this constant value of 0.003 m^3/s. This rapid decrease in the minimum infiltration volume rate emphasizes the saturated hydraulic conductivity as the most important factor in determining the excess runoff hydrographs as observed in the sensitivity analysis.

Incorporating the initial moisture content, the framework also accounts for the antecedent soil moisture content within the soil leading to a more accurate estimate of the soil infiltration capacity prior to a storm event. The framework is also adaptable as it allows for soil properties to be modified depending on the soil type. This flexibility allows for this modeling framework to be extended to systems with soil types other than loamy sand.

Quantifying evapotranspiration (ET) is important in assessing the volume reduction potential of a bioinfiltration system (Hess *et al.* 2015; Wadzuk *et al.* 2015). ET, however, occurs on a much larger timescale compared with infiltration and fluvial geomorphology of a bioinfiltration system. For example, in their study of two bioretention systems over a 2-year span of time, Wadzuk *et al.* (2015) measured an average ET of 6.1 mm/day. In comparison, the median *in situ* saturated hydraulic conductivity rate in this study over a 3-year time span was 8 cm/h (1,900 mm/day). For this reason, ET was ignored in the development of the current framework but should be explored in future work for different types of bioinfiltration installations.

Model validation

The accuracy of a geomorphic model is largely a function of the accuracy of the estimated hydraulic parameters such as flow depths, velocities, and shear stresses. Therefore, it is essential to verify the predicted hydraulic parameters using the observed data. This is particularly important in the absence of quantitative geomorphic change

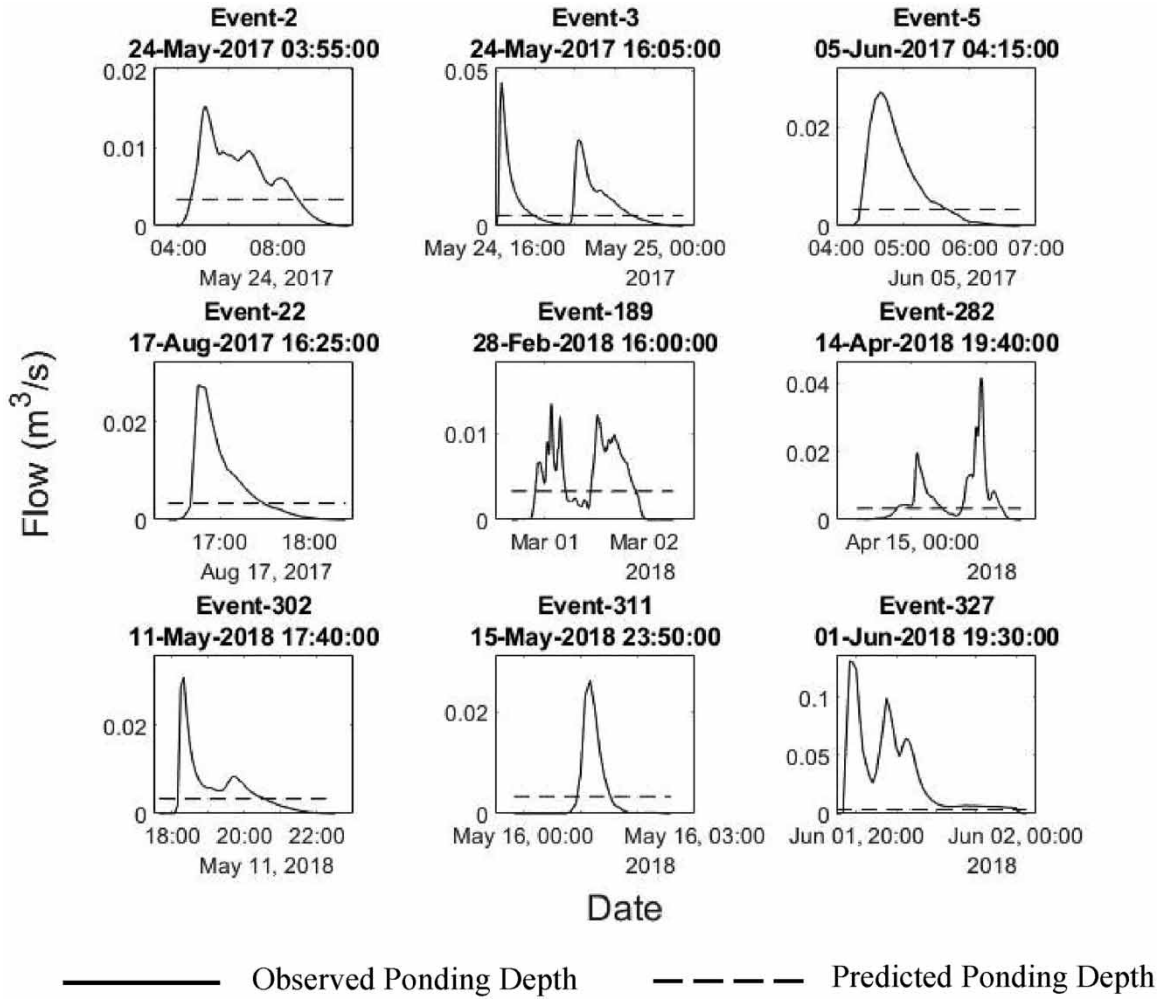

Figure 6 | Green-Ampt infiltration rate estimates for a sample of the individual storm events. The excess runoff, computed as the difference between infiltration and inflow hydrograph, is used for the geomorphic simulation.

data. To evaluate the performance of the proposed framework, the predicted and observed ponding depths for 31 randomly selected significant storm events were compared using data from the B2 gage. Figure 7 represents a sample of comparisons between predicted and observed ponding depth. The full results of these samples, including the NSE and CC, are included in Table S1 (Supplementary Material). As shown, with a few exceptions, such as events 2, 3, 5, and 22, the framework was able to predict the ponding depth with an acceptable level of accuracy. These inconsistencies are driven by an inability to quantify the antecedent moisture content of the media, impacting infiltration estimations.

As seen in Table 1 (or Supplemental Material Table S1), although there were a few instances where the model performed poorly (represented by a negative minimum NSE and low minimum absolute CC), the overall performance of the model on the 31 events was very good (median NSE $= 0.93$ and median CC $= 0.97$).

This high level of prediction accuracy can be attributed to assigning the correct boundary conditions in this study. Specifically, an accurate prediction of the system's ponding depth largely depends on setting the right upstream and downstream boundary conditions. In this study, using water surface elevation data from the B1 gage as the downstream boundary condition was critical for the accuracy of the model. This observation highlights the importance of having a good knowledge of the configuration of the outlet structure when using this framework. It was also notable that the prediction accuracy was better for events where the maximum ponding depth exceeds 0.2 m, such as events 282, 302, 311, and 327 in Figure 7. Saturated soil conditions associated with ponded water allow the system to function more like a river channel with minimal infiltration and with hydraulic conditions controlled by the downstream boundary condition. This was tested using depth data from the pressure transducer at gage B2, located between the inlet and B1 (Figure 2).

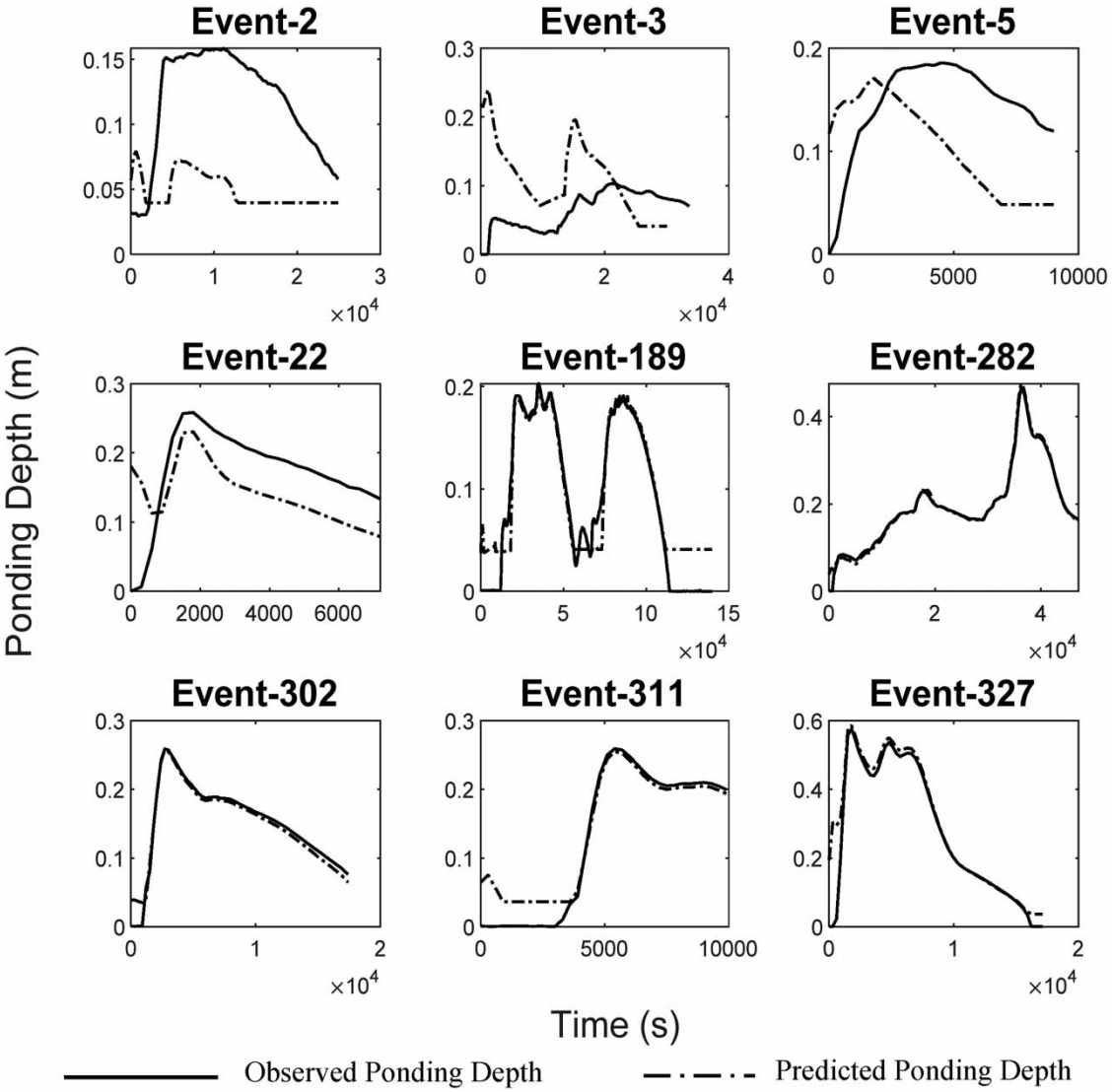

Figure 7 | Comparison of predicted and observed ponding depths within SMP A.

Table 1 | Summary of Nash–Sutcliffe efficiency (NSE) and correlation coefficient for comparison between predicted and observed ponding depths for 31 events

	NSE	Correlation coefficient (absolute)
Median	0.93	0.97
Mean	0.02	0.82
Min	−1.58	0.11
Max	0.99	1.00

Bed shear stress and sediment flux

Bed shear stress determines incipient motion of soil particles. Combined with knowledge of median particle size (d_{50}), the shear stress distribution provides an indication of specific regions within the bioinfiltration system prone to erosion or deposition and the likely evolution of the biofiltration media surface. Figure 8 presents the distribution of shear stresses within the system during the peak of a typical significant storm event (0.03 m^3/s). Based on the median particle size of 0.62 mm, a corresponding critical shear stress of 0.32 Pa was estimated in this study (negligibly small shear stress values were not included). Quantitively assigning a risk level for erosion/sedimentation within a bioinfiltration system can aid maintenance and design. For example, with an

Figure 8 | Shear stress distribution for a typical significant storm event in SMP A.

average shear stress greater than 1.5 Pa, it can be inferred from the shear stress distribution plot that areas with significant shear stress over the critical shear stress such as the central area (in red) will likely be an erosive region. Non-colored areas have low-shear stress and are likely to be depositional. This can be incorporated into identifying maintenance priorities in these areas. This framework provides a means of quantifying the extent of potential maintenance needs which could be included in design to facilitate more sustainable management. Surfaces evolve over time due to erosion and sedimentation, therefore, a dynamic framework for monitoring the evolution of bioinfiltration surfaces is important to understand long-term changes on the bioinfiltration soil media surface. While a dynamic framework is out of the scope of this study, the current study provides the needed foundation for developing such a framework. This distribution of shear stresses and its implications for aggradation and degradation is also confirmed by the sediment flux results subsequently discussed.

The results show that for a typical significant event (0.03 m^3/s) in SMP A, there is not substantial erosion within the system. More likely, there will be deposition in a vast region within the system. The significance of these shear stress distribution results is the ability to identify regions with a high potential for erosion either during design or planning for maintenance of bioinfiltration systems. Sediment flux provides an insight into the rate of mobilization of sediment within the bioinfiltration system. Such knowledge is crucial in predicting sediment erosion and deposition, which can educate long-term maintenance and rehabilitation needs of a bioinfiltration system (DelGrosso *et al.* 2019; Smith *et al.* 2021; Wadzuk *et al.* 2021).

Ideally, this would be validated by repeat topographic field measurements. However, due to the limited timespan of this study physical changes to the surface were too small to measure. Yet, the validation of the hydrologic and hydraulic models provides confidence in sediment flux predictions (Lane 1998; Tamminga & Eaton 2018). Figure 9 shows the sediment flux of SMP A during the peak of a typical significant storm event (0.03 m^3/s) paired with images taken in the field. As expected, the high shear stress locations coincide with the highest sediment fluxes although the rate of soil loss is generally very low. The low sediment loss rate is consistent with the current observation of the site.

SMP A currently shows minor spot erosion and micro-channelization around vegetation but no major erosion within the system except for scouring downstream of the weirs due to relatively higher velocities. It is important to highlight that one limitation of the current framework is the inability to model localized erosion around individual clusters of vegetation and hydraulic structures such as the weirs. It is expected that the vortices around individual vegetation or clusters of vegetation will lead to increased scouring. However, modeling this scenario is outside the scope of this study and may be better suited for more advanced unsteady 3-D hydrodynamic or morphodynamic modeling.

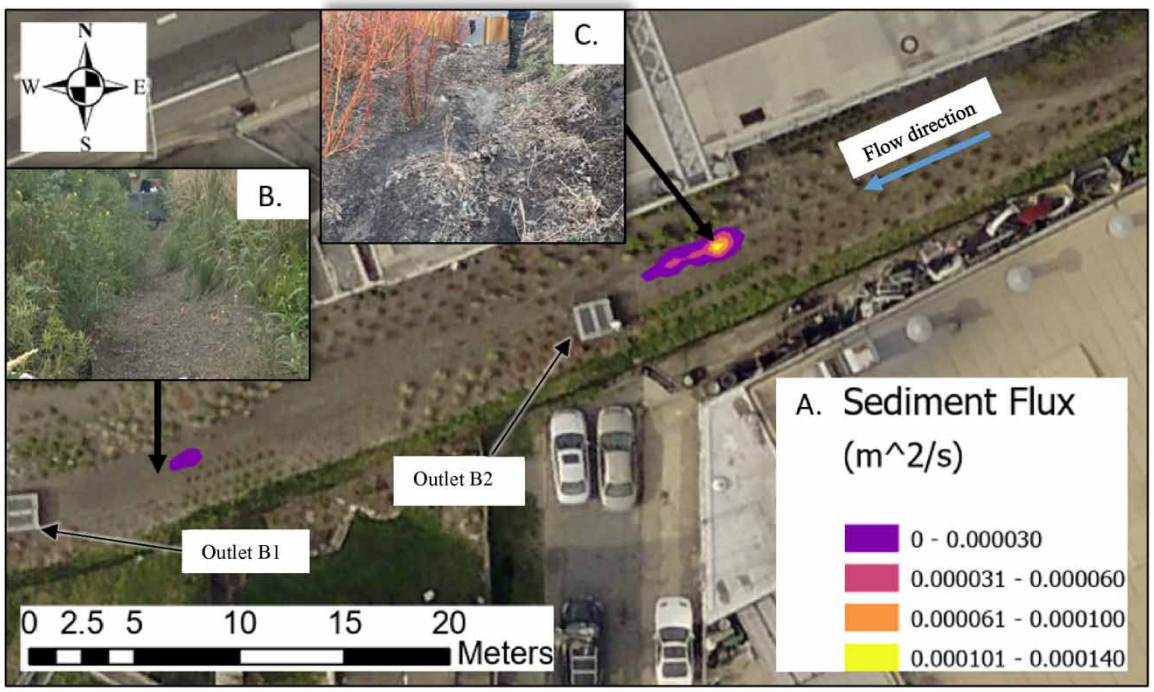

Figure 9 | (a) Sediment flux showing rate of loss of soil within the bioinfiltration. system. (b) Shows an example of deposition. (c) Shows an example of erosion. These images spatially align with the model results.

Limitations

Despite the high level of accuracy achieved comparing the observed hydraulic depth in the pond and predicted pond depth of the bioinfiltration system, this framework has some limitations. As highlighted earlier, the FaSTMECH sediment transport model utilized in this study allows for a single inflow boundary. This presents a challenge when evaluating systems with multiple inlets, like ours. Future studies on this framework must incorporate other transport models with more flexibility to accommodate additional inflow locations.

Another important factor to note is that the current framework assumes that the bioinfiltration media is homogenous. This may be true for engineered system such as a bioinfiltration system. However, caution should be exercised when the framework is being applied to non-homogenous systems or systems where the soil bed has been significantly altered by the introduction of different soil types. Use of the Green-Ampt method allows for input parameters that are easily obtainable from the literature. The limitations of this method, however, are that it may not fully address the spatial variability typical of a bioinfiltration system and only provides an approximate solution to Richard's Equation. The assumptions of an initially uniform moisture content profile and a sharp wetting front may introduce additional errors associated with the use of the Green-Ampt method. Another limitation is the fact that the results only represent the median particle sizes (d_{50}) and thus may not fully capture the dynamics of the entire range of particle sizes within the soil media.

As has been demonstrated in this study, the framework requires a downstream boundary condition to be defined in order for the simulation to proceed. In fact, the accuracy of the results obtained from this framework is largely a function of correctly defining the downstream boundary condition. Additionally, this geometry may not be representative of typical bioinfiltrations systems and as such may not be applicable in every case. Future studies may need to examine the applicability of this model to other systems. Understanding this limitation is important during data collection for using this framework.

CONCLUSIONS

This study introduces a novel framework for spatial prediction of sediment erosion and deposition within a bioswale. By identifying regions of potential high shear stress (erosion) and sediment deposition (sedimentation) maintenance requirements and long-term performance of bioinfiltration systems can be more focused. This has the potential to aid in dynamic maintenance (Wadzuk *et al.* 2021). This study highlights an important, yet

often ignored aspect of low impact development design, which is understanding the evolution of the soil media. Substantial soil loss within soil media impedes the performance of the system by limiting the storage volume capacity of the system and may overwhelm downstream infrastructure with eroded soil material. A good understanding of the dynamics of the soil media morphology helps in predicting and prioritizing future maintenance needs as well as SMP design to minimize impact from excessive erosion or deposition. For large systems, understanding the shear stress distribution and rate of soil loss can have major cost saving implications by knowing which storm events can significantly impact the integrity of the infiltration bed. As nature-based solutions play an increasingly significant role in urban stormwater management, leveraging existing modeling tools for natural systems provides an opportunity for advancing the science and engineering in tangential fields. Enabling the ability to identify areas where deposition and erosion are likely to occur will allow for more efficient and sustainable designs, and aid in identifying the drivers of underperformance or non-performance of systems, since the depositional areas are likely to correspond with areas of reduced infiltration rates.

The current study has introduced a unique method of modeling the hydraulics and morphology of a bioinfiltration system with a high degree of accuracy. This was achieved by combining an existing model, FaSTMECH, with an infiltration model (Green-Ampt). This novel approach allows for an accurate accounting of the high infiltration rates typical of bioinfiltration systems while modeling sediment transport within the system. The proposed framework is unique as it repurposes an existing river model for a bioinfiltration system and provides an inexpensive method for modeling the hydraulics and morphology of systems with high amounts of infiltration using easily accessible open access tools.

In developing the current framework, the most important data requirements include a DEM, k_{sat}, d_{50} of the soil media, inflow hydrograph, and the ponding depth. Of the hydrologic data required for utilizing this modeling framework, downstream ponding depth information appears to be the most critical input. This is because ponding is largely controlled by the configuration of the hydraulic structures. The accuracy of a model, therefore, is highly dependent on a good understanding of the ponding elevations.

While some limitations were identified with FaSTMECH, there are other solvers within the iRIC platform that may have the potential to represent systems more accurately with multiple inlets. This needs to be investigated in future studies. As these tools evolve it will enable testing a range of storm events and infrastructure geometries, providing insight into how sediments move through these systems, potentially impacting their function.

The authors have presented the first known attempt to model morphology and bioinfiltration soil loss in order to identify potential problematic areas within the system where significant erosion or channelization is likely to occur. The bed shear stress and sediment flux outputs of the proposed framework will be a crucial tool for low impact development (LID) engineers and planners in targeting and prioritizing specific regions within a system where failure or underperformance is likely to occur. This framework will also be an effective tool for evaluating design alternatives for minimizing soil loss within a bioinfiltration system.

ACKNOWLEDGEMENTS

The authors would like to thank the Pennsylvania Department of Transportation (PennDOT) for their support and funding. The opinions presented in this publication are those of the authors and do not necessarily express the opinions of the PennDOT. Reference in this report to any commercial product, process, or service, or the use of any trade, firm, or corporation name is for general informational purposes only and does not constitute an endorsement or certification of any kind by the authors. This project is a research initiative of the Villanova Center for Resilient Water Systems. The authors would also like to thank their colleagues on this project, faculty, graduate research assistants, and undergraduate research assistants, in this project for their invaluable insights during the preparation of the manuscript.

DATA AVAILABILITY STATEMENT

Data cannot be made publicly available; readers should contact the corresponding author for details.

CONFLICT OF INTEREST

The authors declare there is no conflict.

REFERENCES

Anim, D. O. & Banahene, P. 2021 Urbanization and stream ecosystems: the role of flow hydraulics towards an improved understanding in addressing urban stream degradation. *Environmental Reviews* **29** (3), 401–414.

Arcement, G. J. & Schneider, V. R. 1989 *Guide for Selecting Manning's Roughness Coefficients for Natural Channels and Flood Plains*. US Geological Survey Water-Supply Paper. Vol. 2339. https://doi.org/10.3133/wsp2339.

Asleson, B. C., Nestingen, R. S., Gulliver, J. S., Hozalski, R. M. & Nieber, J. L. 2009 Performance assessment of rain gardens. *Journal of the American Water Resources Association* **45** (4), 1019–1031. https://doi.org/10.1111/j.1752-1688.2009.00344.x.

Bedient, P. B., Huber, W. C. & Vieux, B. E. 2008 *Hydrology and Floodplain Analysis*. 4th edn. Prentice-Hall Inc, Upper Saddle River, NJ 07458.

Brownlie, W. R. 1981 *Prediction of Flow Depth and Sediment Discharge in Open Channels. Report No. KH-R-43A*. Pasadena, CA.

Chappell, N. A., Tych, W., Chotai, A., Bidin, K., Sinun, W. & Chiew, T. H. 2006 BARUMODEL: combined data based mechanistic models of runoff response in a managed rainforest catchment. *Forest Ecology and Management* **224** (1), 58–80. https://doi.org/10.1016/j.foreco.2005.12.008.

Coustumer, S. L., Fletcher, T. D., Deletic, A., Barraud, S. & Poelsma, P. 2012 The influence of design parameters on clogging of stormwater biofilters: a large-scale column study. *Water Research* **46** (20), 6743–6752. https://doi.org/10.1016/j.watres.2012.01.026.

Davis, A. P., Shokouhian, M., Sharma, H., Minami, C. & Winogradoff, D. 2003 Water quality improvement through bioretention: lead, copper, and zinc removal. *Water Environment Research* **75** (1), 73–82. https://doi.org/10.2175/106143003X140854.

Davis, A. P., Hunt, W. F., Traver, R. G. & Clar, M. 2009 Bioretention technology: overview of current practice and future needs. *Journal of Environmental Engineering* **135** (3), 109–117. https://doi.org/10.1061/(ASCE)0733-9372(2009)135:3(109).

Davis, A. P., Traver, R. G., Hunt, W. F., Lee, R., Brown, R. A. & Olszewski, J. M. 2012 Hydrologic performance of bioretention storm-water control measures. *Journal of Hydrologic Engineering* **17** (5), 604–614. https://doi.org/10.1061/(ASCE)HE.1943-5584.0000467.

DelGrosso, Z. L., Hodges, C. C. & Dymond, R. L. 2019 Identifying key factors for implementation and maintenance of green stormwater infrastructure. *Journal of Sustainable Water in the Built Environment* **5** (3), 1–12. https://doi.org/10.1061/JSWBAY.0000878.

Ebrahimian, A., Wadzuk, B. & Traver, R. 2019 Evapotranspiration in green stormwater infrastructure systems. *Science of the Total Environment* **688**, 797–810.

Garcia, M. H. 2007 *Sedimentation Engineering: Processes, Measurements, Modeling, and Practice*. ASCE, No. 110. Reston, Virginia. https://doi.org/10.1061/9780784408148.ch02.

Gonzalez-Merchan, C., Sylvie, B., Le Coustumer, S. & Fletcher, T. D. 2010 *Monitoring of Clogging Evolution in the Infiltration System Université De Lyon, and Université Lyon Suivi de l ' Évolution de Colmatage Dans Les Ouvrages d ' Infiltration*. pp. 1–10.

Green, W. H. & Ampt, G. A. 1911 Studies on soil physics. *The Journal of Agricultural Science* **4** (1), 1–24. Available from: https://www.cambridge.org/core/services/aop-cambridge-core/content/view/S0021859600001441.

Hammond, M. J., Chen, A. S., Djordjević, S., Butler, D. & Mark, O. 2015 Urban flood impact assessment: a state-of-the-art review. *Urban Water Journal* **12** (1), 14–29.

Harrison, L. R., Dunne, T. & Burch Fisher, G. 2015 Hydraulic and geomorphic processes in an overbank flood along a meandering, gravel-Bed river: implications for chute formation. *Earth Surface Processes and Landforms* **40** (9), 1239–1253. https://doi.org/10.1002/esp.3717.

Hess, A., Wadzuk, B. & Welker, A. 2015 Evapotranspiration and infiltration in rain garden systems. In: *World Environmental and Water Resources Congress 2015: Floods, Droughts, and Ecosystems – Proceedings of the 2015 World Environmental and Water Resources Congress*. pp. 261–270. https://doi.org/10.1061/9780784479162.025.

Homet, K., Kremer, P., Smith, V., Ampomah, R. & Strader, S. M. 2022 Mapping predicted areas of common maintenance impacts to green stormwater infrastructure in Philadelphia, Pennsylvania. *Journal of Sustainable Water in the Built Environment* **8** (3), 05022003. https://doi.org/10.1061/JSWBAY.0000986.

Hosseiny, H. & Smith, V. 2019 Two dimensional model for backwater geomorphology: Darby Creek, PA. *Water* **11** (11), 2204. https://doi.org/10.3390/w11112204.

Hunt, W. F., Lord, W. G. & Smith, J. T. 2020 Determining BMP inspection and maintenance costs for structural BMPs in North Carolina. In *Impacts of Global Climate Change. Proceedings*. https://doi.org/doi:10.1061/40792(173)173.

Jarman, D. S., Faram, M. G., Butler, D., Tabor, G., Stovin, V. R., Burt, D. & Throp, E. 2008 Computational fluid dynamics as a tool for urban drainage system analysis: A review of applications and best practice. In *11th International Conference on Urban Drainage*, 31 August - 5 September 2008, Edinburgh, Scotland.

Jeon, M., Guerra, H. B., Choi, H., Kwon, D., Kim, H. & Kim, L.-H. 2021 Stormwater runoff treatment using rain garden: performance monitoring and development of deep learning-based water quality prediction models. *Water* **13** (24), 3488.

Lane, S. N. 1998 Hydraulic modelling in hydrology and geomorphology: a review of high resolution approaches. *Hydrological Processes* **12** (8), 1131–1150.

Langergraber, G., Haberl, R., Laber, J. & Pressl, A. 2003 Evaluation of substrate clogging processes in vertical flow constructed wetlands. *Water Science and Technology* **48** (5), 25–34. https://doi.org/10.2166/wst.2003.0272.

Lastra, J., Fernández, E., Díez-Herrero, A. & Marquínez, J. 2008 Flood hazard delineation combining geomorphological and hydrological methods: an example in the northern Iberian peninsula. *Natural Hazards* **45** (2), 277–293. https://doi.org/10.1007/s11069-007-9164-8.

Lee, R. S., Traver, R. G. & Welker, A. L. 2016 Evaluation of soil class proxies for hydrologic performance of in situ bioinfiltration systems. *Journal of Sustainable Water in the Built Environment* **2** (4), 1–10. https://doi.org/10.1061/JSWBAY.0000813.

Leopold, L. 1968 Hydrology for urban land planning – a guidebook on the hydrologic effects of urban land use. *Geological Survey Circular* **554**, 1–21. Available from: http://enviro.lclark.edu/resources/Tryon/Water/Hydrology.pdf.

Mailapalli, D. R., Raghuwanshi, N. S. & Singh, R. 2013 Sediment transport model for a surface irrigation system. *Applied and Environmental Soil Science* **2013**, 1–10.

May, C. L. & Pryor, S. 2015 Explaining spatial patterns of mussel beds in a northern California river: the role of flood disturbance and spawning salmon. *River Research and Applications* (32), 776–785. https://doi.org/10.1002/rra.2894EXPLAINING.

McDonald, R., Nelson, J., Paragamian, V. & Barton, G. 2010 Modeling the effect of flow and sediment transport on white sturgeon spawning habitat in the Kootenai River, Idaho. *Journal of Hydraulic Engineering* **136** (12), 1077–1092. https://doi.org/10.1061/(ASCE)HY.1943-7900.0000283.

McGrane, S. J. 2016 Impacts of urbanisation on hydrological and water quality dynamics, and urban water management: a review. *Hydrological Sciences Journal* **61** (13), 2295–2311. https://doi.org/10.1080/02626667.2015.1128084.

McKean, J. & Tonina, D. 2013 Bed stability in unconfined gravel bed mountain streams: with implications for salmon spawning viability in future climates. *Journal of Geophysical Research: Earth Surface* **118** (3), 1227–1240. https://doi.org/10.1002/jgrf.20092.

Nash, J. E. & Sutcliffe, J. V. 1970 River flow forecasting through conceptual models part I – a discussion of principles. *Journal of Hydrology* **10** (3), 282–290. https://doi.org/10.1016/0022-1694(70)90255-6.

Nelson, J. M. 2016 *FaSTMECH Model Notes*. Available from: http://i-ric.org/en/download/get/rFx2Wj.

Nelson, J. 2018 *IRIC Software*.

Nelson, J. M., Bennett, J. P., Wiele, S. M., 2003 Flow and sediment transport modeling. In: *Tools in Geomorphology* (Kondolph, M. & Piegay, H., eds). Wiley and Sons, Chichester, UK, p. 688.

Nelson, J. M., Shimizu, Y., Takebayashi, H. & McDonald, R. R. 2010 The International River Interface Cooperative (IRIC) – public domain software for river modeling. In *Joint Federal Interagency Conference, 2nd*. p. 8. Available from: http://acwi.gov/sos/pubs/2ndJFIC/Contents/3E_Nelson_03_01_10.pdf.

Philadelphia Water Department 2021 *Green Stormwater Infrastructure Planning & Design Manual. Version 3.0.* January 2021. Available from: https://water.phila.gov/gsi/planning-design/manuals.html

Press, J. 2019 Determining the minimum number of single ring infiltration tests required to reliably predict performance of a rain garden. Master's thesis, Dept. of Civil and Environmental Engineering, Villanova University.

Rawls, W. J., Brakensiek, D. L. & Miller, N. 1983 Green-Ampt infiltration parameters from soils data. *Journal of Hydraulic Engineering* **109** (1), 62–70. https://doi.org/10.1061/(ASCE)0733-9429(1983)109:1(62).

Smith, C., Connolly, R., Ampomah, R., Hess, A., Sample-Lord, K. & Smith, V. 2021 Temporal soil dynamics in bioinfiltration systems. *Journal of Irrigation and Drainage Engineering* **147** (11), 04021053. doi:10.1061/(asce)ir.1943-4774.0001617.

Smith, J. S., Winston, R. J., Wituszynski, D. M., Tirpak, R. A., Boening-Ulman, K. M. & Martin, J. F. 2023 Effects of watershed-scale green infrastructure retrofits on urban stormwater quality: a paired watershed study to quantify nutrient and sediment removal. *Ecological Engineering* **186**, 106835. https://doi.org/10.1016/j.ecoleng.2022.106835.

Tamminga, A. & Eaton, B. 2018 Linking geomorphic change due to floods to spatial hydraulic habitat dynamics. *Ecohydrology* **11** (8), e2018.

Tindall, J. A., Kunkel, J. R. & Anderson, D. E. 1999 Unsaturated zone hydrology for scientists and engineers (Vol. 4). Prentice Hall, Upper Saddle River, NJ.

Virahsawmy, H. K., Stewardson, M. J., Vietz, G. & Fletcher, T. D. 2014 Factors that affect the hydraulic performance of raingardens: implications for design and maintenance. *Water Science and Technology* **69** (5), 982–988. https://doi.org/10.2166/wst.2013.809.

Wadzuk, B. M., Hickman, J. M. & Traver, R. G. 2015 Understanding the role of evapotranspiration in bioretention: Mesocosm study. *Journal of Sustainable Water in the Built Environment* **1** (2), 1–7. https://doi.org/10.1061/JSWBAY.0000794.

Wadzuk, B., Gile, B., Smith, V., Ebrahimian, A. & Traver, R. 2021 Call for a dynamic approach to GSI maintenance. *Journal of Sustainable Water in the Built Environment* **7** (2), 02521001.

Waite, I. R., Munn, M. D., Moran, P. W., Konrad, C. P., Nowell, L. S., Meador, M. R., Van Metre, P. C. & Carlisle, D. M. 2019 Effects of urban multi-stressors on three stream biotic assemblages. *Science of the Total Environment* **660**, 1472–1485. https://doi.org/10.1016/j.scitotenv.2018.12.240.

Weiss, P. T. & Gulliver, J. S. 2015 Effective saturated hydraulic conductivity of an infiltration-based stormwater control measure. *Journal of Sustainable Water in the Built Environment* **1** (4), 04015005. https://doi.org/10.1061/JSWBAY.0000801.

Wolman, G. M. & Schick, A. P. 1967 Effects of construction on fluvial sediment, urban and suburban areas of Maryland. *Water Resources Research* **3** (2), 451–464. https://doi.org/10.1029/WR003i002p00451.

Wu, C. C. & Meyer, L. D. 1989 Simulating transport of nonuniform sediment along flatland furrows. *Transactions of the ASAE* **32** (5), 1651–1661.

Yalin, M. S. 1963 An expression for bedload transportation. *Division, ASCE* **89**, 221–250.

Zarzar, C. M., Hosseiny, H., Siddique, R., Gomez, M., Smith, V., Mejia, A. & Dyer, J. 2018 A hydraulic multimodel ensemble framework for visualizing flood inundation uncertainty. *JAWRA Journal of the American Water Resources Association*. https://doi.org/10.1111/1752-1688.12656.

First received 2 March 2023; accepted in revised form 10 August 2023. Available online 25 September 2023